Title
High-performance lithium/sulfur cells with a bi-functionally immobilized sulfur cathode

Authors
Lin, Zhan
Nan, Caiyun
Ye, Yifan
et al.

Publication Date
2014-10-01

DOI
10.1016/j.nanoen.2014.08.003

Peer reviewed

Nano Energy (2014) 9, 408–416

Available online at www.sciencedirect.com

ScienceDirect

journal homepage: www.elsevier.com/locate/nanoenergy

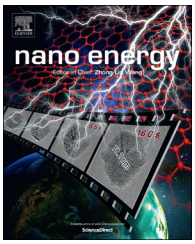

RAPID COMMUNICATION

High-performance lithium/sulfur cells with a bi-functionally immobilized sulfur cathode

Zhan Lin[a,b,1], Caiyun Nan[a,b,c], Yifan Ye[d,e], Jinghua Guo[e,f], Junfa Zhu[d], Elton J. Cairns[a,b,*]

[a]*Department of Chemical and Biomolecular Engineering, University of California, Berkeley, CA 94720, USA*
[b]*Environmental Energy Technologies Division, Lawrence Berkeley National Laboratory, Berkeley, CA 94720, USA*
[c]*Department of Chemistry, Tsinghua University, Beijing 100084, China*
[d]*National Synchrotron Radiation Laboratory, University of Science and Technology of China, Hefei 230029, China*
[e]*Advanced Light Source, Lawrence Berkeley National Laboratory, Berkeley, CA 94720, USA*
[f]*Department of Chemistry and Biochemistry, University of California, Santa Cruz, CA 95064, USA*

Received 9 June 2014; received in revised form 24 July 2014; accepted 6 August 2014
Available online 19 August 2014

KEYWORDS
Lithium/sulfur cell;
Lithium sulfide;
Sulfur composite cathode;
Core-shell nanoparticles;
Lithium sulfide cell;
Carbon coating

Abstract
Lithium/sulfur (Li/S) cells have a theoretical specific energy five times higher than that of lithium-ion (Li-ion) cells (2600 vs. ~500 Wh kg^{-1}). The conventional Li/S cells that use an organic liquid electrolyte are short-lived with low coulombic efficiency due to the polysulfide shuttle. We herein design carbon-coated NanoLi_2S (NanoLi_2S@carbon) composites, which consist of Li_2S nanoparticles as the core and a carbon coating as the shell. The carbon shell prevents the NanoLi_2S core from directly contacting the liquid electrolyte, which improves the performance of Li/S cells to provide longer cycle life and high sulfur utilization. The cyclability of Li/S cells is further enhanced by mixing the core-shell NanoLi_2S@carbon composites with graphene oxide, which chemically immobilizes polysulfides in the cathode through their functional groups. The resulting Li/S cell shows an initial specific discharge capacity of 1263 mAh g^{-1} (normalized to sulfur) at the *C*/10 rate and a capacity retention of 65.4% after 200 cycles. The capacity decay mechanism during cycling is also characterized in detail using near edge X-ray absorption fine structure (NEXAFS) spectra.

*Corresponding author at: Department of Chemical and Biomolecular Engineering, University of California, Berkeley, CA 94720, USA.
E-mail address: ejcairns@lbl.gov (E.J. Cairns).
[1]Zhan Lin now is professor at Zhejiang University in Hangzhou, China.

http://dx.doi.org/10.1016/j.nanoen.2014.08.003
2211-2855/

Introduction

The depletion of fossil fuels and the effects of green house gases have aroused great interest in developing high energy density storage systems throughout the world [1-4]. The lithium/sulfur (Li/S) cell, consisting of lithium metal as the anode and elemental sulfur as the cathode, has been considered as the next-generation energy storage system for electric vehicles and large-scale grids. Based on the conversion reaction of

$$16Li + S_8 \rightarrow 8Li_2S \quad (1)$$

the Li/S cell can supply a theoretical specific energy of 2600 Wh kg^{-1}, which is five times greater than that of the lithium-ion (Li-ion) cell [5-7].

The conventional Li/S cell uses an organic liquid electrolyte. During discharge, elemental sulfur is reduced to form soluble polysulfides (e.g., Li_2S_x, $4 \leq x \leq 8$), which can dissolve into the organic liquid electrolyte. Since the elemental sulfur and its final discharge product Li_2S are neither electronically nor ionically conductive, the operation of Li/S cells depends on the dissolution of polysulfides in the liquid electrolyte [8-13]. However, the high solubility of polysulfides in the organic electrolyte represents a significant challenge in conventional Li/S cells, *i.e.*, the polysulfide shuttle. The polysulfide shuttle migrates sulfur species from the cathode to the anode, resulting in the loss of active material, short cycle life of the sulfur-based electrode, and low coulombic and energy efficiencies [14,15]. In order to prevent the polysulfide shuttle and improve the cycling performance, the construction of a solid, essentially insoluble sulfur cathode is a necessity in the conventional liquid-electrolyte Li/S systems. Moreover, cycling the metallic lithium anode in the organic liquid electrolyte also remains a problem. During recharge, the metallic lithium forms dendrites, which can penetrate the separator and short the cell [16-19].

Currently much Li/S research focuses on using an elemental sulfur cathode because of its high specific capacity (1675 mAh g^{-1}) and light weight. The prevention of the polysulfide shuttle by a conductive polymer coating is a common method for protecting the sulfur particles. Lithium sulfide (Li_2S) has been studied as the prelithiated sulfur electrode in Li/S cells because of its high melting point (1372 °C) and favorably high specific capacity (1166 mAh g^{-1}) [20-22]. The Li_2S cathode supplies lithium and may avoid the direct use of a metallic lithium anode [23,24]. The possible combination of the Li_2S cathode with a Si or Sn anode can dramatically enhance the energy density of traditional rechargeable lithium cells [8,25]. However, bulk Li_2S has low electronic and ionic conductivity as low as 10^{-14} and 10^{-13} S cm^{-1}, respectively; and it has been considered to be an electrochemically inactive material.

To promote the electrochemical activity of Li_2S, herein we report a solid sulfur cathode prepared by an environmentally benign synthesis of nanostructured Li_2S (NanoLi_2S) via reacting elemental sulfur with lithium triethylborohydride ($LiEt_3BH$) in tetrahydrofuran (THF). The NanoLi_2S is coated with conductive carbon by heat-treatment of the Li_2S particles with a thin coating of polyacronitrile (PAN) polymer on the surface to form a core-shell structure (NanoLi_2S@carbon). This structure not only enhances the conductivity, but also inhibits the dissolution of sulfur species for improved cycling performance. The cyclability of carbon-coated NanoLi_2S is further improved by mixing it with graphene oxide (GO-NanoLi_2S@carbon), which chemically constrains polysulfides within the cathode by the functional groups (such as hydroxyl, epoxide, carbonyl and carboxyl groups). The resulting Li/S cell shows an initial specific discharge capacity of 1263 mAh g^{-1} (normalized to sulfur) at the rate of *C*/10 with a capacity retention of 65.4% after 200 cycles, which makes it a promising cathode material for Li/S cells.

Results and discussion

Figure 1a shows the synthesis schematic of core-shell carbon-coated NanoLi_2S as cathode materials for Li/S cells. First, NanoLi_2S was prepared by reacting elemental sulfur (S) with lithium triethylborohydride ($LiEt_3BH$) in tetrahydrofuran (THF), Eq. (2):

$$S + 2Li(CH_2CH_3)_3BH \rightarrow Li_2S\downarrow + 2\,(CH_2CH_3)_3B + H_2\uparrow \quad (2)$$

During the reaction, aggregates of Li_2S nanoparticles precipitated from the THF solution; and the particles are not very uniform in size since particle aggregates are found (Figure 1b). However, we can synthesize uniform NanoLi_2S spheres by modifying the preparation procedure [26]. The collected NanoLi_2S was washed, centrifuged, and dried at 140 °C under vacuum for 2 h prior to use. Before carbon coating, the NanoLi_2S was heat-treated at 500 °C under Ar for 0.5 h, and a thin carbon layer of 2-3 nm was formed on the surface of the NanoLi_2S. Carbon-coated NanoLi_2S composites were prepared by the pyrolysis of a PAN coating (from DMF solution) on the NanoLi_2S. After heat treatment at 600 °C in Ar for 1 h, a much thicker carbon layer is found on the surface of NanoLi_2S, e.g., the thickness of the coating layer is 20-30 nm when the carbon content is 10 wt% (Figure 1c).

Figure 2a shows the X-ray diffraction (XRD) patterns of as-prepared NanoLi_2S, NanoLi_2S after heat-treatment at 500 °C, and core-shell NanoLi_2S@carbon composites. The XRD patterns of the NanoLi_2S are identical to those of bulk Li_2S (JCPDS card no. 23-0369). These peaks are identified as a pure phase of Li_2S: 27.2° (111), 31.6° (200), 45.1° (220), 53.5° (311), and 56.0° (222), respectively. The XRD peaks of NanoLi_2S show significant peak broadening compared to those of the bulk Li_2S. The estimated crystallite size is 20-30 nm, which is much smaller than that of the bulk Li_2S particles (i.e., the particle size is ~1 μm). After heat-treatment at 500 °C, the peak widths become much narrower, which is due to the crystal growth of NanoLi_2S. The average size of the NanoLi_2S aggregates is 500 nm in diameter after heat-treatment. However, when the Nano-Li_2S was further coated with carbon by the pyrolysis of the PAN polymer on its surface, the average size of the NanoLi_2S is preserved. The carbon coating procedure does not change the particle size of the NanoLi_2S with heat-treatment at 600 °C.

Raman spectra of NanoLi_2S, NanoLi_2S after heat-treatment at 500 °C and core-shell NanoLi_2S@carbon are shown in Figure 2b. Significant peaks are found in the wavenumber range from 250 to 2000 cm^{-1} in the Raman

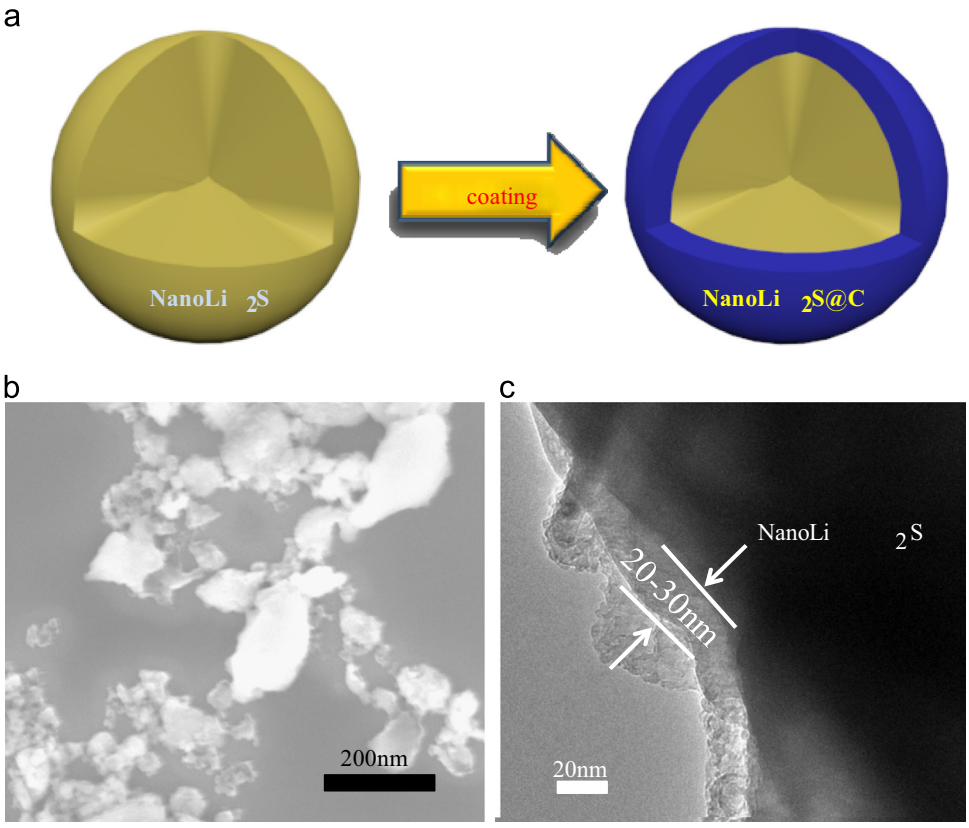

Figure 1 Synthesis and characterization of NanoLi$_2$S and core-shell NanoLi$_2$S@carbon composites. (a) The synthesis schematic of core-shell NanoLi$_2$S@carbon composites. (b) The SEM image of NanoLi$_2$S. (c) TEM image of core-shell NanoLi$_2$S@carbon composites.

spectra. The strong peak for NanoLi$_2$S at 375 cm^{-1} is evidence of stretching vibrations of the Li-S bond, and the peaks between 700 and 1500 cm^{-1}are identified with the C-H, C-S, S-H and S-O bonds [27,28] and reflect the existence of organic residues. After heat-treatment in Ar at 500 °C for 0.5 h, these peaks are gone due to the carbonization of the organic residue (the color of NanoLi$_2$S changed from light yellow to gray). The peak at 1335 cm^{-1} is assigned to the disordered graphite structure (D-band), and the peak at 1587 cm^{-1} (G-band) corresponds to a splitting of the E2g stretching mode of graphite, which reflects the structural intensity of the sp2-hybridized carbon atoms. The G- and D- bands in the Raman spectrum suggest a typical amorphous carbon coating on the surface of NanoLi$_2$S. The relative intensity of the NanoLi$_2$S peak indicates the thickness of the carbon coating. After heat-treatment at 500 °C and carbon coating, the diffraction peaks of NanoLi$_2$S disappear due to the layer of carbon on the NanoLi$_2$S. The peaks of both XRD and Raman spectra confirm the core-shell structure of carbon-coated NanoLi$_2$S composite, which is consistent with the TEM image in Figure 1c. This carbon coating not only allows electron and ion transports within it, but also prevents the NanoLi$_2$S from directly contacting the liquid electrolyte, which mitigates the polysulfide shuttle and improves the cycling performance.

To determine the electrochemical properties and reversibility, the cyclic voltammogram (CV) of Li/S cells was obtained by using NanoLi$_2$S@carbon composites as the cathode in the liquid electrolyte (0.18 M $LiNO_3$+1 M LiTFSI in PYR_{14}TFSI/DME/DOL, 2:1:1 by volume), as shown in Figure 3a. When scanning upward from the open circuit voltage (OCV) on the 1st cycle, two broad oxidation peaks between 3.0 and 4.0 V are caused by lithium extraction from NanoLi$_2$S. In the conventional Li/S cell, the oxidation potential to form sulfur species is always around 2.5 V. The higher oxidation potentials here are caused by low conductivity and poor lithium extraction kinetics of NanoLi$_2$S during the electrochemical reaction. When scanning to lower potentials, two clear reduction peaks around 2.4 and 2.0 V are found: the one around the 2.4 V is comprised of the transformation of S to higher-order Li$_2$S$_x$ ($4 \leq x \leq 8$), and the other one at around 2.0 V was caused by further reduction of the higher-order lithium polysulfides to lower-order Li$_2$S$_x$ ($x \leq 4$), and to Li$_2$S. After scanning downward to 1.5 V, one clear oxidation peak is found, which confirms the good reversibility of sulfur species such as Li$_2$S$_x$ (x=1 or 2). The same situations are also found at the 2nd and 3rd cycle; therefore, the potential range of 1.5-2.8 V vs. Li/Li$^+$ was chosen for further evaluation of the cycling performance.

Figure 3b shows the typical constant current charge-discharge profiles of NanoLi$_2$S@carbon cathodes when using the cut-off potentials of 1.5-3.75 V for the 1st cycle at C/10, and 1.5-2.8 V for the following cycles at C/2 ($1C$=1166 mA g^{-1} Li$_2$S). At the 1st charge, the voltage keeps increasing until the cut-off voltage of 3.75 V, which confirms the continuous lithium extraction from NanoLi$_2$S. For the charge-discharge curves of the Li/S cell at the 3rd cycle, two voltage plateaus at 2.4 and 2.0 V during the discharge procedure, which correspond to the reduction of

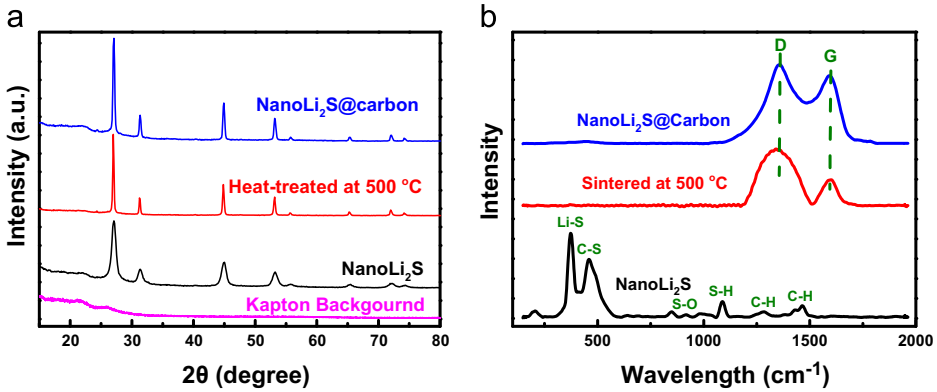

Figure 2 Characterization of $NanoLi_2S$ and core-shell $NanoLi_2S$@carbon composites. (a) XRD patterns and (b) Raman spectra of $NanoLi_2S$, $NanoLi_2S$ after heat-treatment at 500 °C, and core-shell $NanoLi_2S$@carbon composites.

long chain polysulfides (S_x^{2-}, $4 \leq x$) and short chain polysulfides (S_x^{2-}, $x \leq 4$), are found. The ratio of the first plateau at 2.4 V to the second plateau at 2.0 V is about 1:3, which indicates the possible blockage of the polysulfide shuttle. The plateau at high voltage (2.4 V) is also found during the charging process; all of these results are consistent with the peaks observed in the CV profiles.

Excellent cycling performance was demonstrated when using the $NanoLi_2S$ and core-shell $NanoLi_2S$@carbon composites as cathode materials for Li/S cells, as shown in Figure 3c. The core-shell $NanoLi_2S$@carbon cathode demonstrates an initial discharge specific capacity of 902 mAh g^{-1} at $C/10$ (unless otherwise noted, the capacities hereafter are normalized to the weight of Li_2S; however, the capacities are also shown in terms of the weight of sulfur for reference), which is 77.4% of its theoretical specific capacity. The core-shell $NanoLi_2S$@carbon cathode was tested at the 2nd cycle at $C/2$, which has the capacity of 761 mAh g^{-1}. After 60 cycles, the capacity decays to 582 mAh g^{-1}, which is about 1/2 of its theoretical maximum. Though the initial discharge capacity of $NanoLi_2S$ is higher than that of $NanoLi_2S$@carbon at $C/2$ (810 vs. 761 mAh g^{-1}), it quickly decays to 582 mAh g^{-1} after only 37 cycles. Moreover, the coulombic efficiency of the $NanoLi_2S$@carbon cathode is also much higher than that of the $NanoLi_2S$ cathode (~99% vs. 98.4%, not shown in the figure). Both the cycling performance and coulombic efficiency of $NanoLi_2S$ are improved by the carbon coating on the surface, which not only enhances the conductivity of the bulk material but also prevents direct contact with the organic electrolyte. As a result, the polysulfide shuttle is greatly inhibited.

The cycling performance of $NanoLi_2S$@carbon composite was further improved by mixing with GO (GO-$NanoLi_2S$@carbon). The initial discharge capacity of the GO-$NanoLi_2S$@carbon cathode is 757 mAh g^{-1} at $C/2$, which gradually decays to half of its theoretical maximum after 100 cycles; after 200 cycles, the capacity decays to 441 mAh g^{-1}, which demonstrates a capacity retention of 58.3%. When the GO-$NanoLi_2S$@carbon cathode was cycled at the low rate of $C/10$, the capacity recovers to about 1/2 of its theoretical maximum, i.e., 575 mAh g^{-1}. Further improvement in the cycling performance may be achieved by modification of the functional groups on the GO surface, which chemically immobilize the polysulfides in the cathode during cycling. The good protection achieved by using carbon coating and GO is confirmed by the high coulombic efficiency (Figure 3d). The initial coulombic efficiency of the GO-$NanoLi_2S$@carbon cathode is about 93%; after that it has a coulombic efficiency of ~99.5% during the entire cycling process, which is much higher than those of the $NanoLi_2S$@carbon cathode and the $NanoLi_2S$ cathode. It should be noted that the coulombic efficiency decreases to ~75% after 100 cycles at the low rate of $C/10$. Though the capacity is much higher when the $C/10$ rate was chosen, the polysulfide shuttle is more severe at low cycling rates than that at high rates. However, after a few cycles at $C/2$, the coulombic efficiency recovers back to ~99.5%. Such a high coulombic efficiency indicates the suppression of the polysulfide shuttle, which has been shown to be the main cause of low coulombic efficiency in the traditional Li/S cells when using an organic liquid electrolyte [29,30]. When using GO-$NanoLi_2S$@carbon as the cathode material for Li/S cells at high current densities, excellent rate capability is achieved (Figure 3e). The cell shows a reversible capacity of 360 mAh g^{-1} at $2C$ after 50 cycles at various rates, and further cycling at a low rate of $C/5$ shows a recovery of the reversible capacity to 587 mAh g^{-1}. Figure 3e illustrates the benefits of carbon coating in the improvement of conductivity, and the GO in chemically constraining the polysulfides within the cathode.

As has been well documented, the soluble polysufides transport sulfur species from the sulfur cathode to the Li anode, where they can chemically react with metallic Li and represent active material loss and low coulombic efficiency (<90%). Considering the good cycling performance (65.4% capacity retention after 200 cycles) and high coulombic efficiency (~99.5%) when using GO-$NanoLi_2S$@carbon composites as cathode material, we believe that the important role of protection can be provided by both carbon coating and GO usage. Therefore, we carried out a simple bench-top test of the polysulfide dissolution and composition measurement of the sulfur species in the cathode to study the effectiveness of the carbon coating in protecting against sulfur loss. The polysulfide dissolution test when using $NanoLi_2S$ and $NanoLi_2S$@carbon composites for comparison is shown in Figure 4a. The solution is the liquid electrolyte

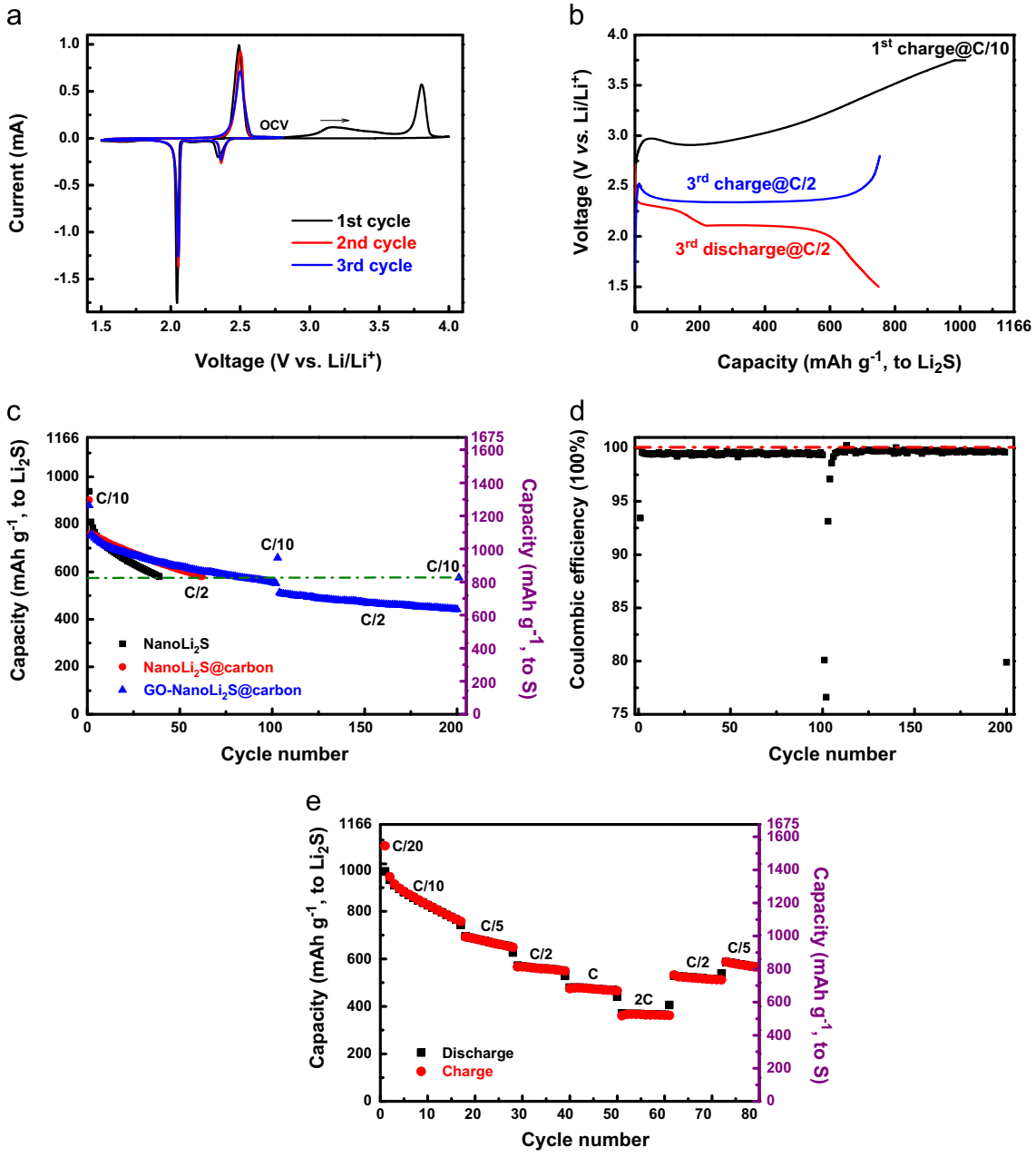

Figure 3 Electrochemical evaluations of NanoLi$_2$S, NanoLi$_2$S@carbon composites, and GO-NanoLi$_2$S@carbon composites as cathode materials for Li/S cells (1C=1166 mAg^{-1} Li$_2$S). (a) Cyclic voltammogram of NanoLi$_2$S@carbon composites for the potential range of 1.5–4.0 V vs. Li/Li$^+$ using scan rate of 0.025 mV s^{-1}. (b) Representative voltage profiles of NanoLi$_2$S@carbon cathode at the 1st and 3rd cycles. (c) Cycling comparisons of NanoLi$_2$S, NanoLi$_2$S@carbon, and GO-NanoLi$_2$S@carbon cathodes, respectively, at the *C*/2 rate. (d) The coulombic efficiency of GO-NanoLi$_2$S@carbon cathode. (e) The rate capability of GO-NanoLi$_2$S@carbon cathode.

used for the cell cycling. Sulfur was added to the solution first; and its amount is determined by the reaction of

$$7S + Li_2S \rightarrow Li_2S_8 \quad (3)$$

When adding the NanoLi$_2$S to the solution, the color of the solution immediately became dark-brown, which indicated the formation of Li_2S_8. In comparison, there is no color change when adding the NanoLi$_2$S@carbon composite to the solution. The color is nearly unchanged after standing for 6 h, which indicates the protection of NanoLi$_2$S from the organic electrolyte by the carbon coating. There was color change overnight (20 h), which indicates the gradual formation of polysulfides.

GO was further chosen to constrain the polysulfides in the cathode during cycling; and the sulfur anchoring is illustrated in Figure 4b by using NEXAFS spectroscopy in the TFY mode. There are six peaks found in the NEXAFS spectra of the NanoLi$_2$S/GO composite. The peaks at 2470.80 and 2472.37 eV were attributed to the transition of S 1s to π^* state of linear polysulfides and the transition from the S

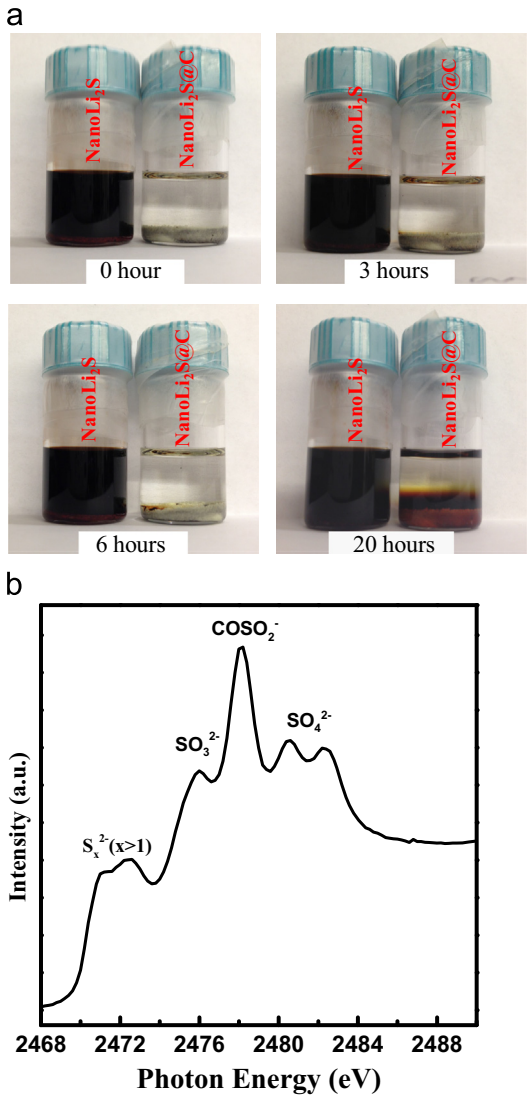

Figure 4 The study of protection the mechanism by using GO-NanoLi$_2$S@carbon as cathode material. (a) The polysulfide dissolution test when using NanoLi$_2$S and NanoLi$_2$S@carbon composite for comparison. The color changes of these two samples containing the same amount of Li$_2$S$_8$ by using the liquid electrolyte were recorded by camera with time. (b) NEXAFS spectroscopy of S Kedge of the NanoLi$_2$S/GO composites from the TFY signal.

1s core level to the S-S π^* state of linear polysulfides (S_x^{2-}, $x>1$); the peaks located at 2476.17, 2478.12, 2480.32, and 2482.42 eV are assigned to the σ^* state of Li$_2$S, the S^{2-} σ^* state and/or the SO_3^{2-} σ^* state, the $COSO_2^-$ σ^* state, and the SO_4^{2-} σ^* state, respectively [31-33]. Comparing with the peaks of NanoLi$_2$S only (not shown in the figure), there should be two peaks observed at 2472–2473 eV; however, the peak at 2473.32 eV may overlap with the broad peak located at 2472.37 eV [32,33]. Most of the Li$_2$S was bonding with oxygen functional groups of the GO sheet by forming S-O, and part of the Li$_2$S was transformed to Li$_2$S$_x$ ($x>1$). The above evidence shows the strong chemical bonding between the NanoLi$_2$S and GO, which can chemically immobilize sulfur species in the cathode.

In order to study the capacity loss mechanism during cycling, NEXAFS spectra were used to characterize the GO-NanoLi$_2$S@carbon composites at the end of charge/discharge after different numbers of cycles. Since NanoLi$_2$S was used as the S cathode material, we first charged the cell. Figure 5a shows the total-fluorescence-yield (TFY) S K edge NEXAFS spectra of the cathode material after five different numbers of charge/discharge cycles and stopped in the charged state. After the first charge, several significant changes were observed, which reflect the evolution of the S chemical species: the disappearance of the peak at 2470.80 eV, the decay of the peak at 2476.00 eV, the appearance of peaks at 2470.34 and 2473.89 eV, and the intensification of the SO_4^{2-} peak. The peaks at 2472.37 and 2473.89 eV are originated from the S-S bonding and the C-S bonding, respectively [33-35]. The small peak at 2470.34 eV is associated with the bonding of S to GO, but the specific transition involved is still an open question [34,35]. These S species are active species that are involved in the

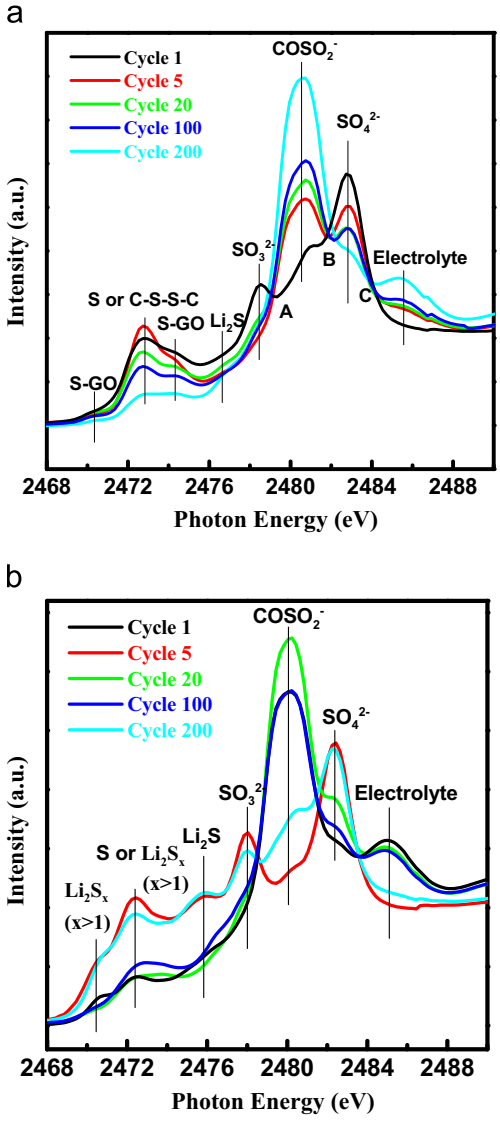

Figure 5 TFY S K edge NEXAFS spectra of the cathode materials with five different charge/discharge cycles and stopped at the (a) charged and (b) discharged states.

charge/discharge process. According to the Li_2S_x ($x>1$) and Li_2S peak intensity evolution located at 2470.80 and 2476.00 eV, the Li_2S_x ($x>1$) species were fully oxidized to elemental S_8 while the Li_2S was partly oxidized during the first charge. In the meantime the S species were bonded to the GO sheets and formed C-S bonds, which help to immobilize sulfur in the cathode.

With the increasing numbers of charge/discharge cycles, several significant peak intensities evolve. First, the peak intensity originating from the S_8 and/or C-S-S-C became stronger after 5 cycles, due to the conversion of more Li_2S to active S species during the first few cycles. With increasing cycle numbers, the active S peak intensity decreased, which might be caused by polysulfide dissolution. Second, the peak intensities of SO_3^{2-} and SO_4^{2-} continuously decay, while the peak intensity of the $COSO_2^-$ specie is always increasing. The interesting point is that all the spectra go through three points marked as A, B and C in the figure, which are attributed to phase transition phenomena. The SO_3^{2-} and SO_4^{2-} were most likely to convert to the $COSO_2^-$ specie within the cycling process, which are all unexpected products during cycling. Finally, there is a peak located even higher than where SO_4^{2-} is, which is assigned to the remaining electrolyte. The intensity of this peak increases with the increasing cycle number as this specie comes from the electrolyte and stays on the cathode surface, which is also confirmed by total-electron-yield (TEY) spectra (Figure S1a and S1c). As the TEY mode is more surface-sensitive than the TFY mode, these species are more likely to accumulate on the cathode surface and form a new layer at the cathode/electrolyte interface. This layer hinders the diffusion of Li-ions within the cathode, leading to the lower utilization of active sulfur species and subsequent capacity fading during cycling.

TFY and TEY S K-edge NEXAFS of cathode materials recorded after different numbers of cycles and stopped in the discharged state are shown in Figures 5b, S1b, and S1d, respectively. After the first discharge, the peak intensity of lithium polysulfides increases while the intensity of the Li_2S peak decreases. This indicates that the elemental S_8 was mostly reduced to Li_2S_x ($x>1$) during discharge. As a result, the proposed electrochemical reaction of $2Li+xS \leftrightharpoons Li_2S_x$, ($1 \leq x < 8$) is demonstrated. Comparing with the fresh cathode material, the ratio of the peak at 2470.80 eV to the peak at 2472.34 eV is much smaller at the discharged state. We propose two reasons: (1) the S_8 and C-S-S-C bondings remain, and (2) the cathode materials can only be discharged to Li_2S_x($x>1$) [33]. With the increase in cycle number, the evolutions of the S species are similar to those of the charged samples: (1) the decay of Li_2S_x, (2) the accumulation of an unexpected layer (SO_3^{2-}, SO_4^{2-}, $COSO_2^-$, and electrolyte), and (3) the phase transition from SO_3^{2-} and SO_4^{2-} to $COSO_2^-$. Therefore, with the decay of the active sulfur species (Li_2S_x) during charge/discharge and the accumulation of the surface layers, the overall capacity fading mechanism during the cycling was illuminated.

Conclusion

In summary, high-performance Li/S cells were developed by combining core-shell NanoLi$_2$S@carbon with GO as the cathode material. The carbon coating prevents NanoLi$_2$S from contacting the liquid electrolyte, which greatly improves the cycling performance of Li/S cells. The cells using the carbon coating show superior cyclability to those using uncoated NanoLi$_2$S. The cycling performance of Li/S cells using NanoLi$_2$S@carbon was further improved by mixing the NanoLi$_2$S@carbonwith GO. The functional groups on the surface of GO chemically absorb the polysulfides within the cathode, which prevents them from dissolving in the electrolyte and subsequently from reacting with the lithium anode. The protection mechanisms from carbon coating and the functional groups of GO were studied in detail, and confirms the great inhibition of the polysulfide shuttle during cycling. The Li/S cell shows an initial specific discharge capacity of 1263 mAh g^{-1}(normalized to sulfur) at the rate of $C/10$ and capacity retention of 65.4% after 200 cycles. The decay mechanism during cycling is characterized and discussed in detail and confirmed by using NEXAFS spectra. This research provides a new approach for designing novel Li_2S cathodes for Li/S cells with excellent cycling performance and sulfur utilization.

Experimental section

Chemicals and reagents

Sulfur (S), lithium sulfide (Li_2S), 1 M superhydride ($LiEt_3BH$) in THF, carbon black (CB), bis(trifluoromethane)sulfonimide lithium salt (LiTFSI, 99.95% trace metals basis), N-methyl-2-pyrrolidone (NMP), 1,3-dioxolane (DOL), and dimethoxyethane (DME) were purchased from Sigma-Aldrich and were used without further purification.

Synthesis

The NanoLi$_2$S was synthesized through a solution-based reaction of elemental sulfur powder with 1.0 M $Li(CH_2CH_3)_3BH$ solution in THF. The sulfur first dissolved and then precipitated out as nanoparticles of NanoLi$_2$S. The collected NanoLi$_2$S was washed, centrifuged, and heat-treated at 140 °C under vacuum for 2 h prior to use. Before carbon coating, the NanoLi$_2$S was heat-treated at 500 °C under Ar for 0.5 h to convert any organic residue to carbon. The carbon coated NanoLi$_2$S was prepared by the pyrolysis of the NanoLi$_2$S with polyacronitrile (PAN) at 600 °C in Ar. The PAN was dissolved in the DMF solution, and then added the weighed NanoLi$_2$S and stirred for 1 h. After the evaporation of the solvent, the mixture of NanoLi$_2$S with polyacronitrile (PAN) was carbonized at 600 °C in Ar. The carbon content was measured by the weight gain of NanoLi$_2$S before and after heat-treatment, which was found to be ~10 wt%.

GO-NanoLi$_2$S@carbon was prepared by adding certain amounts of NanoLi$_2$S@carbon (carbon content is ~10%) and GO (GO content in is also ~10 wt%) into THF, which was sonicated for 2 h and then dried for further use. The cathode slurry was prepared by mixing GO-NanoLi$_2$S@carbon (75 wt%), carbon black (20 wt%), and PVP (5 wt%) in NMP. After 0.5 h sonication, the cathode slurry was coated onto carbon paper (the current collector). This electrode was assembled with the lithium metal foil into a traditional coin

cell. The cell was assembled using the GO-NanoLi_2S@carbon as the cathode, 0.18 M $LiNO_3$ + 1 M LiTFSI in PYR_{14}TFSI/DME/DOL (2:1:1 by volume) as the liquid electrolyte, and metallic lithium foil as the anode. The electrode loading was 2.3 mg mixture cm^{-2}, or 1.5 mg Li_2S cm^{-2}.

The bench-top color measurement was tested by using the same amount of Li_2S_8 ($Li_2S + 7S \rightarrow Li_2S_8$) in the liquid electrolyte. The sulfur was first added into the liquid electrolyte. During the testing, the NanoLi_2S and Nano-Li_2S@carbon were added into the liquid electrolyte, respectively. The color changes of these two samples were recorded by camera with time.

Electrochemical evaluation and structure characterization

Coin cells were used to evaluate the cycling performance. Carbon papers with the thickness of $\sim$100 μm were used as the current collector. Charge and discharge were carried out using a Maccor 4000 series cell tester at a current density of 0.2 mA cm^{-2} ($C/10$) between the cut-off potentials of 1.5-2.8 V vs. Li/Li^+. The current densities of 0.4 ($C/5$) and 0.75 ($C/2.5$) mA cm^{-2} were applied to measure the rate capability. The calculation of specific charge/discharge capacities is based on the mass of lithium sulfide and sulfur content.

The structures of the cathode electrode before and after cycling were examined using a field emission STEM (Hitachi HF-3300) at 15 kV. The elemental mapping of the samples was also taken using STEM. X-ray diffraction (XRD) analysis was performed at a PANalyticalX'pert PRO2-circle X-ray diffractometer with a CuKα radiation ($\lambda \approx 1.5418$ Å). Raman spectroscopy was recorded from 500 to 200 cm^{-1} on a Renishaw Confocal Micro Raman spectrometer at room temperature.

X-ray absorption fine structure (NEXAFS) spectra

The original Li_2S/GO composites were prepared by in-situ depositing NanoLi_2S onto the surface of GO. The cathode materials were taken out from the coin cells in the glove box under Argon. The samples were transferred to the beamline in the Advanced Light Source at Lawrence Berkeley National Laboratory. S K edge NEXAFS spectra were collected in bending magnet beamline 9.3.1. Total electrons yield signals (TEY) were collected by monitoring the offset sample drain current, and the total fluorescence yield (TFY) signals were collected by a silicon drift detector. NEXAFS is a powerful technique for identifying and characterizing the chemical and bonding characteristics of materials. S K-edge NEXAFS spectra correspond to the transitions from S 1s to 3p orbital and are sensitive to the chemical environment varies. The NEXAFS peaks at absorption photon energies were corresponded to different S-based species.

Acknowledgments

This work was sponsored by Robert Bosch LLC through the Bosch Energy Research Network Grant no. 16.11.BS11, and by the University of California-Berkeley, Energy and Climate Research Innovation Seed Fund. The Advanced Light Source is supported by the Director, Office of Science, Office of Basic Energy Sciences, of the U.S. Department of Energy under Contract no. DE-AC02-05CH11231. We thank Dr. Tev Kuykendall for his support in the Molecular Foundry of LBNL. Y.F.Y. and J.F.Z. greatly acknowledge the financial support from the National Natural Science Foundation of China (Grant no. U1232102).

Appendix A. Supporting information

Supplementary data associated with this article can be found in the online version at http://dx.doi.org/10.1016/j.nanoen.2014.08.003.

References

[1] P.G. Bruce, S.A. Freunberger, L.J. Hardwick, J.M. Tarascon, Nat. Mater. 11 (2012) 19-29.
[2] J.M. Tarascon, M. Armand, Nature 414 (2001) 359-367.
[3] L.W. Ji, Z. Lin, Y. Li, S.L. Li, Y.Z. Liang, O. Toprakci, Q.A. Shi, X.W. Zhang, Polymer 51 (2010) 4368-4374.
[4] L.W. Ji, Z. Lin, M. Alcoutlabi, O. Toprakci, Y.F. Yao, G.J. Xu, S.L. Li, X.W. Zhang, RSC Adv. 2 (2012) 192-198.
[5] X.L. Ji, K.T. Lee, L.F. Nazar, Nat. Mater. 8 (2009) 500-506.
[6] N. Jayaprakash, J. Shen, S.S. Moganty, A. Corona, L.A. Archer, Angew. Chem. Int. Ed. 50 (2011) 5904-5908.
[7] Z. Lin, Z. Liu, W. Fu, N.J. Dudney, C. Liang, Adv. Funct. Mater. 23 (2013) 1064-1069.
[8] Y. Yang, M.T. McDowell, A. Jackson, J.J. Cha, S.S. Hong, Y. Cui, Nano Lett. 10 (2010) 1486-1491.
[9] L.F. Xiao, Y.L. Cao, J. Xiao, B. Schwenzer, M.H. Engelhard, L.V. Saraf, Z.M. Nie, G.J. Exarhos, J. Liu, Adv. Mater. 24 (2012) 1176-1181.
[10] S.S. Zhang, J.A. Read, J. Power Sources 200 (2012) 77-82.
[11] J.C. Guo, Y.H. Xu, C.S. Wang, Nano Lett. 11 (2011) 4288-4294.
[12] S. Xin, L. Gu, N.H. Zhao, Y.X. Yin, L.J. Zhou, Y.G. Guo, L.J. Wan, J. Am. Chem. Soc. 134 (2012) 18510-18513.
[13] L.W. Ji, M.M. Rao, H.M. Zheng, L. Zhang, Y.C. Li, W.H. Duan, J. H. Guo, E.J. Cairns, Y.G. Zhang, J. Am. Chem. Soc. 133 (2011) 18522-18525.
[14] Y.V. Mikhaylik, J.R. Akridge, J. Electrochem. Soc. 151 (2004) A1969-A1976.
[15] C.D. Liang, N.J. Dudney, J.Y. Howe, Chem. Mater. 21 (2009) 4724-4730.
[16] A.M. Stephan, K.S. Nahm, Polymer 47 (2006) 5952-5964.
[17] J.F.M. Oudenhoven, L. Baggetto, P.H.L. Notten, Adv. Energy Mater. 1 (2011) 10-33.
[18] Z. Lin, Z. Liu, W. Fu, N.J. Dudney, C. Liang, Angew. Chem. Int. Ed. 52 (2013) 7460-7463.
[19] Z. Lin, Z. Liu, N.J. Dudney, C. Liang, ACS Nano 7 (2013) 2829-2833.
[20] Y. Yang, G.Y. Zheng, S. Misra, J. Nelson, M.F. Toney, Y. Gui, J. Am. Chem. Soc. 134 (2012) 15387-15394.
[21] Z.C. Yang, J.C. Guo, S.K. Das, Y.C. Yu, Z.H. Zhou, H.D. Abruna, L.A. Archer, J. Mater. Chem. A 1 (2013) 1433-1440.
[22] S. Jeong, D. Bresser, D. Buchholz, M. Winter, S. Passerini, J. Power Sources 235 (2013) 220-225.
[23] D. Aurbach, J. Power Sources 89 (2000) 206-218.
[24] B. Scrosati, J. Garche, J. Power Sources 195 (2010) 2419-2430.
[25] J. Hassoun, Y.K. Sun, B. Scrosati, J. Power Sources 196 (2011) 343-348.
[26] C. Nan, Z. Lin, H. Liao, M.-K. Song, Y. Li, E.J. Cairns, J. Am. Chem. Soc. 136 (2014) 4659-4663.

[27] R.E. Barletta, B.N. Gros, M.P. Herring, J. Raman Spectrosc. 40 (2009) 972–981.
[28] L. Zhang, L.W. Ji, P.A. Glans, Y.G. Zhang, J.F. Zhu, J.H. Guo, Phys. Chem. Chem. Phys. 14 (2012) 13670–13675.
[29] D. Marmorstein, T.H. Yu, K.A. Striebel, F.R. McLarnon, J. Hou, E.J. Cairns, J. Power Sources 89 (2000) 219–226.
[30] J. Shim, K.A. Striebel, E.J. Cairns, J. Electrochem. Soc. 149 (2002) A1321–A1325.
[31] J. Gao, M.A. Lowe, Y. Kiya, H.D. Abruña, J. Phys. Chem. C 115 (2011) 25132–25137.
[32] F. Jalilehvand, Chem. Soc. Rev. 35 (2006) 1256–1268.
[33] M.U.M. Patel, I. Arčon, G. Aquilanti, L. Stievano, G. Mali, R. Dominko, Chem. Phys. Chem. 15 (2014) 894–904.
[34] A. Dey, M. Chow, K. Taniguchi, P. Lugo-Mas, S. Davin, M. Maeda, J.A. Kovacs, M. Odaka, K.O. Hodgson, B. Hedman, E.I. Solomon, J. Am. Chem. Soc. 128 (2005) 533–541.
[35] L. Zhang, L. Ji, P.-A. Glans, Y. Zhang, J. Zhu, J. Guo, Phys. Chem. Chem. Phys. 14 (2012) 13670–13675.

Zhan Lin received his Ph.D. in Fiber and Polymer Science at the North Carolina State University in 2010. After that, he worked as Postdoctoral Research Associate at Oak Ridge National Laboratory and Postdoctoral Fellow at University of California-Berkeley/Lawrence Berkeley National Laboratory from 2011 to 2013. In January 2014, he returned to China under the support of "Thousand Youth Talents Program", and become a professor in Department of Chemical and Biological Engineering at Zhejiang University. His research interests focus on nanostructured materials for Electrochemical Energy Storage and Conversion, including lithium-sulfur batteries, lithium-ion batteries, fuel cells, and solar cells.

Caiyun Nan was a visiting researcher under the supervision of Prof. Elton J. Cairns at the University of California, Berkeley, from 2012 to 2014. She received her Ph.D. degree in Inorganic Chemistry from Tsinghua University in 2014 and now works in the Department of Chemistry at Beijing Normal University. Her research interests focus mainly on synthesis and application explorations of nano-materials for lithium-sulfur batteries and lithium ion batteries.

Yifian Ye received his Bachelor's degree from the Department of Chemical Physics at University of Science and Technology of China in 2011. He is currently pursuing his Ph.D. under the supervision of Prof. Junfa Zhu at National Synchrotron Radiation Laboratory at University of Science and Technology of China. He is currently a visiting student at Dr. Jinghua Guo's group at Advanced Light Source, Lawrence Berkeley National Laboratory. His research interests mainly focus on the applications of Synchrotron based probing methods in energy science, such as organic solar cell, organic light-emitting diode and Li-S batteries.

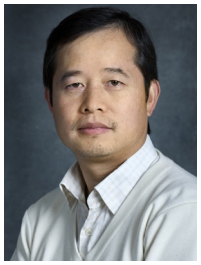

Jinghua Guo is a career staff scientist at the Advance Light Source, Lawrence Berkeley National Laboratory, and adjunct professor in the Department of Chemistry and Biochemistry, University of California, Santa Cruz. He obtained his Ph.D. degree at the Uppsala University, Uppsala, Sweden, in 1995. He is one of the world's leading experts in the field of in situ/operando soft X-ray spectroscopy research. His research interest focuses on energy science research including electronic structure and charge transfer in energy-conversion and energy-storage materials and devices.

Junfa Zhu received in Ph.D. in the Department of Chemical Physics, University of Science and Technology of China (USTC) in 1999. After several years working in the Institute of Experimental Physics, Johannes Kepler Universität Linz, Austria (3/2000–5/2001), Lehrstuhl für Physikalische Chemie II, Friedrich-Alexander-Universität Erlangen-Nürnberg, Germany (6/2001-9/2003), and Department of Chemistry, University of Washington, WA, USA (10/2003–11/2006), he returned to USTC in December, 2006, and become a professor at National Synchrotron Radiation Laboratory, USTC under the support of "Hundred Talent Program" of Chinese Academy of Sciences. His research interests mainly focus on in-situ studies of surface and interface structures and properties of functional materials using advanced surface science techniques including synchrotron radiation soft X-ray spectroscopies.

Elton J. Cairns University of California, Berkeley, and Lawrence Berkeley National Laboratory Elton J. Cairns received his B.S. in Chemistry and B.S. in Chemical Engineering at the Michigan Technological University, and his Ph.D. at the University of California, Berkeley. He currently serves as Professor of the Graduate School in Chemical Engineering, University of California, Berkeley, and Faculty Senior Scientist, Lawrence Berkeley National Laboratory. Dr. Cairns has published in the areas of electrochemical kinetics, batteries, fuel cells, molten salts, liquid metals, thermodynamics, surface chemistry, catalysis, and transport phenomena. His current research includes lithium/sulfur cells, lithium ion cells, and electrocatalysts for fuel cells.